Journal of Alloys and Compounds 509 (2011) 5515–5524

Contents lists available at ScienceDirect

Journal of Alloys and Compounds

journal homepage: www.elsevier.com/locate/jallcom

An in situ neutron diffraction study of the thermal disproportionation of the Zr_2FeD_5 system

M.P. Pitt[a,b,*], L.K.W. Pitt[b,c], H. Fjellvåg[c], B.C. Hauback[b]

[a] Queensland Micro and Nanotechnology Centre, Griffith University, Brisbane 4111, Australia
[b] Institute for Energy Technology, P.O. Box 40, 2027 Kjeller, Norway
[c] Centre for Materials Science and Nanotechnology, Department of Chemistry, University of Oslo, P.O. Box 1126, 0318 Blindern, Norway

ARTICLE INFO

Article history:
Received 11 February 2011
Received in revised form 21 February 2011
Accepted 23 February 2011
Available online 1 March 2011

Keywords:
Intermetallics
Nuclear reactor materials
Metal hydrides
Phase transitions
Neutron diffraction

ABSTRACT

The Zr_2FeD_5 system has been annealed to 680 °C under ultra high vacuum, and studied in situ by neutron diffraction. The system disproportionates through three distinct regions in temperature. Initially, the tetragonal Zr_2FeD_5 (*P4/ncc*) is retained up to 330 °C, while steadily depleted of D. From 330 °C to 530 °C, a complex multi-phase disproportionation occurs, with the production of cubic ZrD_2, tetragonal ZrD_2, tetragonal Zr_2FeD_5 (*I4/mcm*), and growth of the intermetallic $ZrFe_2$. At the beginning of the 330–530 °C period, the total atom count from quantitative phase analysis (QPA) indicates the formation of amorphous (a-) $Zr_{56}Fe_{44}$. By 530 °C, QPA and peak breadth analysis indicate that ca. 2/3rd of the sample is consumed as very small nanocrystals (<150 Å coherence length) of strained ZrD_2. From 530 °C to 680 °C, the cubic ZrD_2 is almost entirely consumed and depleted of D to form the final mixture of the intermetallic phases Zr_3Fe and $ZrFe_2$. QPA of the final intermetallic mixture yields a Zr:Fe ratio greater than that observed in either the arc melted alloy or the initial Zr_2FeD_5 deuteride, indicating that a ca. $Zr_{71}Fe_{29}$ amorphous component was present in the initial arc melted alloy. According to the total atom count by QPA, crystallisation of the Fe richer amorphous $Zr_{56}Fe_{44}$ phase formed at 330 °C begins at ca. 530 °C, and later by 680 °C, all amorphous phases have completely crystallised to yield a 70.77:26.75:2.47 mol.% mixture of Zr_3Fe:$ZrFe_2$:ZrD_{2-x}.

1. Introduction

The $Zr_{1-x}Fe_x$ system is an important alloy system for the nuclear industry, based on the tritium gettering properties of the Zr_2Fe intermetallic [1–6]. The commercial SAES St 198 alloy typically used for non-evaporable hydrogen isotope gettering is predominantly crystalline Zr_2Fe, which forms a very stable hydride, Zr_2FeH_5, with very low plateau pressure at ambient temperature, ca. 1 Pa [7]. Zr_2Fe has also been proposed as an outer safety layer in high pressure hydrogen storage tanks to avoid hydrogen embrittlement and micro cracking of the tank [8]. Amorphous (a-) phases can also be formed from the $Zr_{1-x}Fe_x$ system over a very wide Fe composition range (ca. $0.27 < x_{Fe} < 0.79$) (mechanically milled alloys) [9,10], and >90 at.% Fe in melt spins [11] and thin films [12,13], and are of great interest for their unique magnetic properties.

The crystalline Zr_2Fe intermetallic exists in a small high temperature range in the binary phase diagram, 780–951 °C, with a very narrow range of Zr composition, ca. 0.5 at.% Zr [14], being metastable at room temperature, and only able to be stabilised by the absorption of hydrogen. The Zr_2Fe intermetallic is typically metastabilised at room temperature by rapid quenching from the melt. There exist many quenching techniques, from extremely rapid at 10^6 K/s, such as melt spinning, enabling the production of predominantly bulk amorphous alloys [11], to slower techniques, such as arc melting, typically 10^1 K/s, producing predominantly crystalline alloys. Due to a large gradient of cooling rate between free sample surface (10^1 K/s) and the Cu hearth (up to 10^6 K/s), arc melted samples are typically inhomogeneous, multi-phase [1], and may retain a minor amorphous component [15], which is why arc melted samples are typically flipped and re-melted several times [16–18], or post annealed to ensure homogeneity. Amorphous Zr_2Fe is quite stable, displaying a crystallisation temperature (T_{cryst}) >700 °C for mechanically alloyed material [10], and an onset of crystallisation of ca. 400–430 °C for melt spun material [11,19], defined by a rapid increase in resistivity which peaks at ca. 630 °C, indicating crystallisation and subsequent growth of Zr_2Fe crystallites evolves over a 200 °C span in temperature. Zr_2Fe crystallises with the $CuAl_2$ structure type, and initially forms very fine and well dispersed 2–3 nm nanocrystals [19]. It is reported in [20] that amorphous Zr_2Fe can absorb a small amount of hydrogen, 0.2–0.7 wt.%H, which increases T_{cryst} by ca. 40 K. Crystalline Zr_2Fe can absorb deuterium up to a composition of Zr_2FeD_5, which possesses a tetragonal unit cell in space group *P4/ncc* [18]. The crystalline Zr_2FeH_5 hydride

* Corresponding author at: Queensland Micro and Nanotechnology Centre, Griffith University, Brisbane 4111, Australia.
E-mail address: mark.pitt@gmail.com (M.P. Pitt).

0925-8388/$ – see front matter © 2011 Elsevier B.V. All rights reserved.
doi:10.1016/j.jallcom.2011.02.129

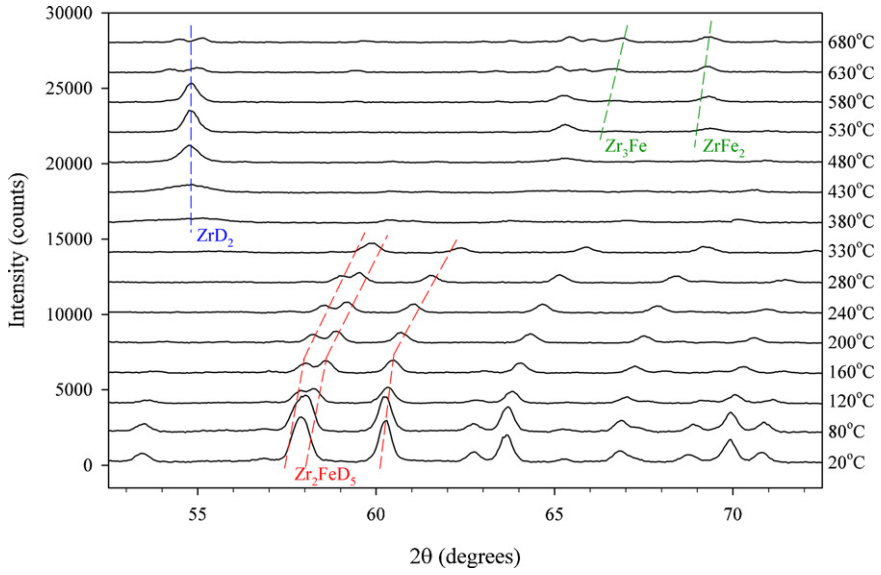

Fig. 1. Raw neutron diffraction data series from 20 to 680 °C, zoomed from 53 to 73° 2θ. Reflections from Zr_2FeD_5, ZrD_2, Zr_3Fe and $ZrFe_2$ are visible, indicated by the dashed lines.

forms part of the greater Zr_2MHx family (M = Ni, Cu, Co, Fe, etc.), all of which display unique crystallographic properties upon hydriding, such as the dislocated monoclinic $Zr_2CuD_{4.71}$ system [21], or the unique triclinic $Zr_2NiD_{4.8}$ structure [22].

Hydrogenation of Zr_2Fe can produce several phases dependent on the temperature used. When charged at 10^3 to 8×10^4 Pa H_2 pressure at <400 °C, it is reported in [16] that a single Zr–Fe hydride is formed, but that above 400 °C, ZrH_2 and $ZrFe_2$ are produced. A $Zr_2FeH_{4.5}$ composition is reported in [17] after hydriding at 0.5–5 atm H_2 at 250 K. Hydrogenation of the SAES St 198 getter at temperatures >350 °C report decomposition of Zr_2FeD_x into ZrD_2 and possibly $ZrFe_2$ [23]. It is also suggested in [23] that formation of ZrD_2 may render the getter irreversible. It was demonstrated in [24,25] for both Zr_2Fe and Zr_3Fe respectively, that if the intermetallics are deuterided above the critical temperature for disproportionation, and significant quantities of ZrD_2 are formed, the material can be recovered at <973 K by releasing D from ZrD_2 under ultra high vacuum. In both cases, the original Zr_2Fe and Zr_3Fe compositions are completely re-formed at high temperature. Such reformation represents an example of the so called Hydrogenation-Disproportionation-Desorption-Recombination (HDDR) process [26], otherwise referred to as vacuum annealing recovery. As such, any capacity decay in Zr_2Fe based tritium getters induced by operating them above 350–400 °C and producing ZrT_2 can be recovered by this annealing process. Recent diffraction studies of the disproportionation of Zr_2FeH_5 have identified $ZrFe_2$ and $ZrH_{1.8}$ after absorption at 500 °C, and Zr_3Fe, $ZrFe_2$ and $ZrH_{1.8}$ after desorption to 800 °C [27]. The desorbed sample could not be reproportionated. In [4], it was noted that disproportionation of Zr_2Fe alloys (including SAES St 198) occurred during hydriding above 400 °C, and that ZrH_x formation could be observed.

In this paper, we follow the disproportionation mechanism of a fully deuterated sample of Zr_2FeD_5 under ultra high vacuum as a function of temperature by in situ neutron diffraction.

2. Experimental procedure

Zr lumps (99.8% purity) and Fe lumps (99.95% purity) were obtained from Goodfellow. The elements were Ar arc melted in the stoichiometric ratio 2:1 in a water cooled Cu hearth. The button was flipped and re-melted six times to obtain homogenous Zr_2Fe. The alloy was crushed under Ar, and activated at 450 °C under ultra high vacuum for 1 h. The alloy was packed in a 6 mm silica-glass tube, and placed in a shielded furnace at the diffractometer sample position. The silica tube is connected to a Sieverts apparatus, which was used to deuteride the sample at room temperature under 1 bar, to a composition of $Zr_2FeD_{4.7}$ by manometry. In situ powder neutron diffraction experiments were carried out using the PUS diffractometer [28] at the JEEP II reactor at Kjeller, Norway. A total of 15 patterns were collected from room temperature up to 680 °C. Monochromated neutrons with $\lambda = 1.5550$ Å were obtained from a Ge (5 1 1) focussing monochromator. The detector unit consists of two banks of seven position-sensitive ^{3}He detectors, each covering 20° in 2θ (binned in 0.05° steps). Data was collected in the 2θ range 10–130°. Neutron diffraction patterns were analysed by the Rietveld method using RIETICA [29]. Diffraction lineshape profiles were fitted with a full Voigt function, with the instrumental shape determined by a NIST Al_2O_3 standard. Quantitative phase analysis (QPA) has been performed on the diffraction data collected at each temperature.

3. Results and discussion

By visual inspection of our raw neutron diffraction data series zoomed over 53–73° 2θ in Fig. 1, we can observe most of the phases involved in the Zr_2FeD_5 disproportionation phase transition. The characteristic Zr_2FeD_{5-x} reflections (1 4 1)/(1 2 3) and (2 4 0) at ca. 58.00 and 60.24° 2θ can be observed to shift to higher 2θ as a function of temperature, indicating unit cell contraction with temperature, suggesting the release of deuterium up to at least 330 °C, after which the phase is no longer easily observed. Past 330 °C, we can observe the formation of cubic ZrD_2 ((2 2 0) at 54.71° 2θ), which is initially very broad, suggesting growth starts from small nanocrystals. By 530 °C, the formation of Zr_3Fe ((2 4 1)/(1 7 1) at 66.49° 2θ) and $ZrFe_2$ ((1 1 5) at 69.27° 2θ) can be observed. Further Rietveld refinement reveals the presence of tetragonal ZrD_2. Fig. 2(a)–(c) shows the Rietveld fits at 20 °C, 380 °C, and 680 °C. Fit quality varies from $\chi^2 = 1.96$–2.96.

Figs. 3 and 4 give an overview of the complete Zr_2FeD_5 disproportionation phase transition, with Fig. 3 showing the global crystalline D/Zr ratio (by Rietveld QPA) of the sample as a function of temperature, and Fig. 4 showing the crystalline phase proportions as a function of temperature. As indicated in each figure, the phase transition can be broken into three distinct regions of temperature, characterised by (i) the depletion of D from tetragonal Zr_2FeD_5 from 20 to 330 °C, (ii) a complex multiple phase region from 330 to 530 °C, where *P*4/*ncc* Zr_2FeD_{5-x} transforms to *I*4/*mcm* Zr_2FeD_{5-x}, nanocrystalline cubic ZrD_2 appears and consumes ca. 2/3rd of the sample, and $ZrFe_2$ alloy growth begins, and (iii) an alloy growth period from 530 to 680 °C, where significant Zr_3Fe growth occurs by ZrD_2 consumption, yielding the final products Zr_3Fe and $ZrFe_2$. In

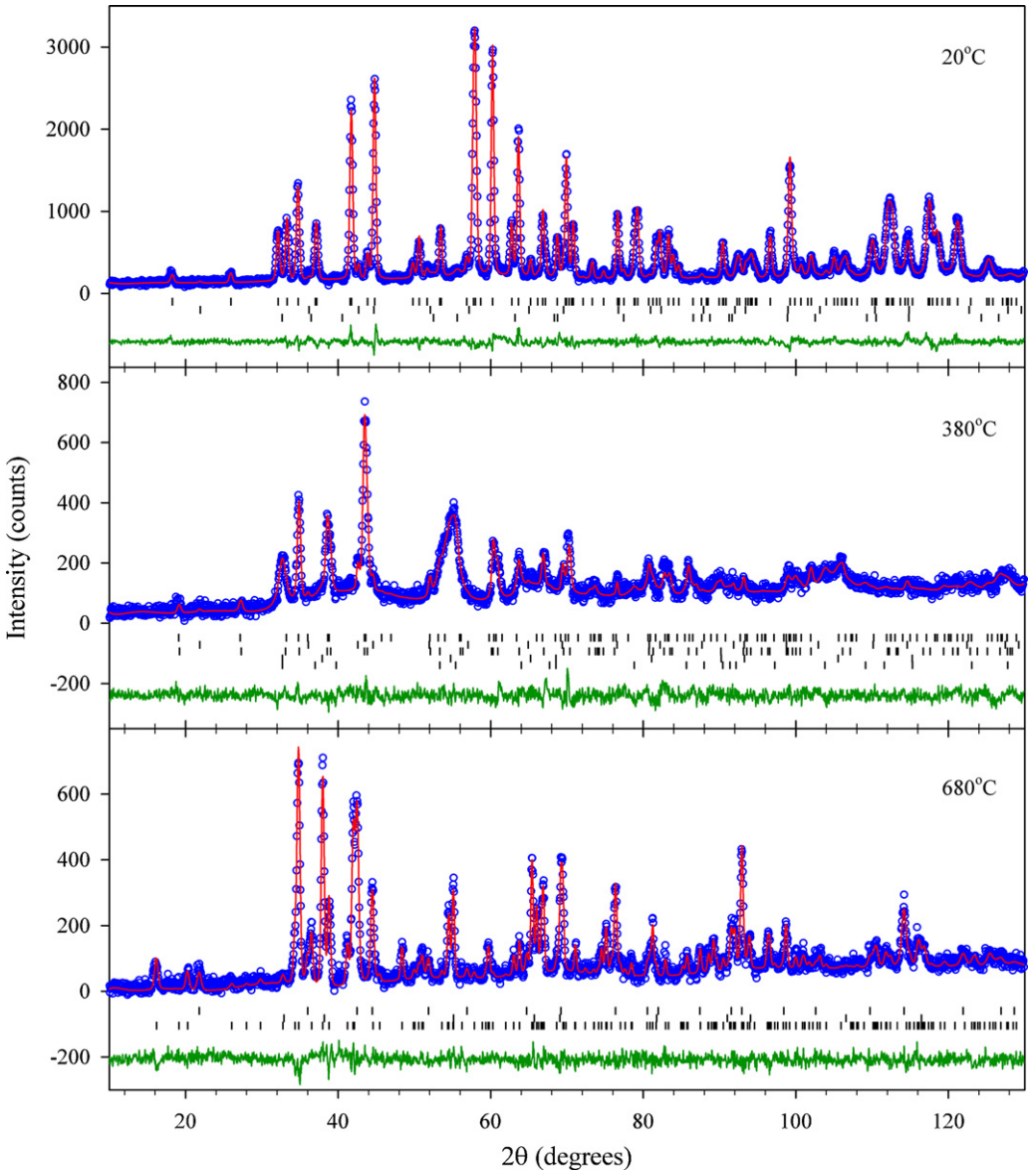

Fig. 2. Rietveld fits from top to bottom, 20 °C, 380 °C and 680 °C. Open circles represent the raw data, with the solid line through them representing the calculation. The difference profile is the solid line below the pattern. Reflection markers, top to bottom 20 °C: *P*4/*ncc* Zr_2FeD_{5-x}, $ZrFe_2$, and *I*4/*mmm* ZrD_2; 380 °C: *P*4/*ncc* Zr_2FeD_{5-x}, $ZrFe_2$, *I*4/*mcm* Zr_2FeD_{5-x}, $Fm\bar{3}m$ ZrD_{2-x} and *I*4/*mmm* ZrD_2; 680 °C: $ZrFe_2$, $Fm\bar{3}m$ ZrD_{2-x} and Zr_3Fe.

the following discussion, we will study the phase transition in detail in each of the three characteristic regions of temperature defined above, and follow the behaviour of the unit cell and D occupancy of each phase, and describe how the various phases react with each other.

3.1. Deuterium depletion from tetragonal *P*4/*ncc* Zr_2FeD_5 from 20 to 330 °C

In this region of temperature, the starting *P*4/*ncc* Zr_2FeD_5 phase has a molar proportion of ca. 91.4%, with minor phases, tetragonal *I*4/*mmm* ZrD_2 (6.1 mol.%) and cubic $Fd\bar{3}m$ $ZrFe_2$ (2.5 mol.%). The phase proportion of Zr_2FeD_5 does not change significantly until after 280 °C. Initially, the room temperature *P*4/*ncc* Zr_2FeD_5 phase possesses a completely ordered D sublattice, with full occupation of 4b (Zr_4 tetrahedra) and 16g (Zr_3Fe tetrahedra) sites. The 16g site is one split half of the 32m site in the parent Zr_2Fe structure, and as discussed in [18], only one half of the original 32m site is occupied with D, which avoids face sharing tetrahedra and short D–D distances. In [30], it is observed that at lower D content, the *P*4/*ncc* Zr_2FeD_{5-x} phase transforms to the tetragonal *I*4/*mcm* Zr_2FeD_{5-x} phase, and the D ordering is removed, and partial occupancy of the 32m and 16l (Zr_4 tetrahedra) sites occurs. In this sense, there are four sites available to D, 32m = 16g + 16g, 4b, 16l = 16g, and 16k (Zr_2Fe_2 tetrahedra). For example, all four of these sites are partially occupied with D in the *I*4/*mcm* $Zr_2NiD_{4.4}$ structure type [22]. The 16k position has not typically been observed to take D for the *I*4/*mcm* Zr_2FeD_{5-x} phase [18], and as such, we utilise four potential sites in the D depleted *P*4/*ncc* Zr_2FeD_{5-x} structure, referred to as D1 (4b Zr_4), D2 (16g = 32m/2 Zr_3Fe), D3 (16g = 32m/2 Zr_3Fe), and D4 (16g = 16l Zr_4). To avoid short D–D distances between face sharing tetrahedra of the split 16g sites (D2 and D3), any occupancy (occ) of the typically empty D3 site must be less than any occupancy decrease of the typically full D2 site, i.e. $occ_{D3} \leq 1\text{-}occ_{D2}$.

As can be noted from Fig. 3, there is a significant loss of D from the sample of ca. 1.6 D/Zr ratio up to 330 °C. For the *P*4/*ncc* Zr_2FeD_{5-x} phase, this is equivalent to a change in composition of Zr_2FeD_5 to ca. $Zr_2FeD_{1.8}$. No D release occurs from the minor tetragonal

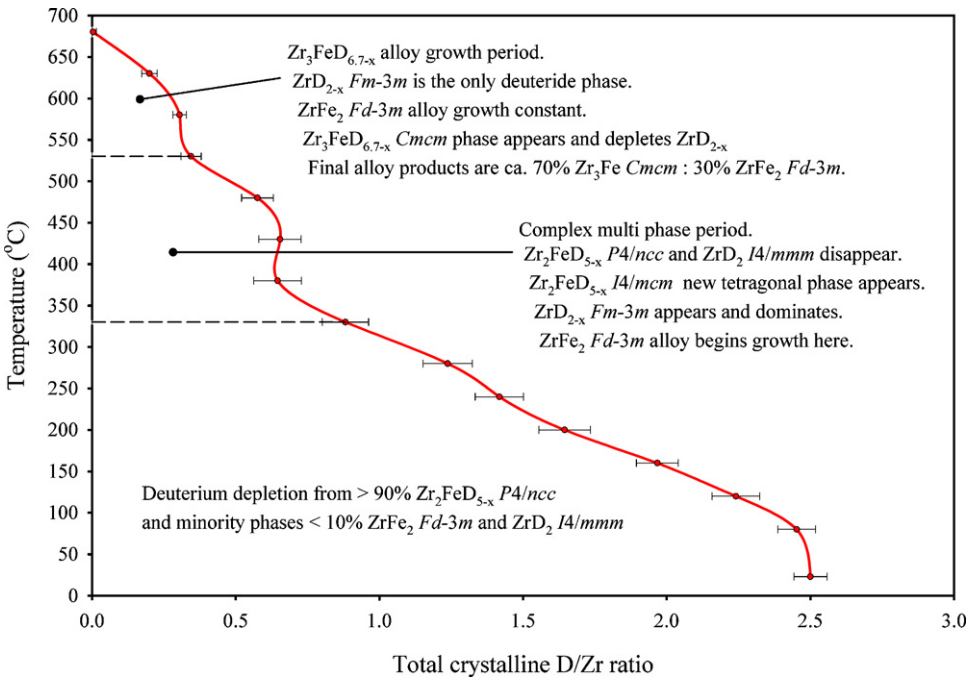

Fig. 3. The crystalline D/Zr ratio (by Rietveld QPA) of the sample as a function of temperature from 20 to 680 °C.

*I*4/*mmm* ZrD_2 phase during this period, so we can expect significant reductions in D site occupancies in the *P*4/*ncc* Zr_2FeD_{5-x} structure, consistent with the shift to lower d-spacing of the Zr_2FeD_{5-x} reflections in Fig. 1. Fig. 5 shows the D occupancies of every phase during the complete phase transition. The D1 (4b Zr_4) and D2 (16g = 32m/2 Zr_3Fe) sites of the *P*4/*ncc* Zr_2FeD_{5-x} structure are significantly reduced to ca. 40% and 8% respectively from their originally full occupancies. From ca. 150 °C onward, the D3 (16g = 32m/2 Zr_3Fe) and D4 (16g = 16l Zr_4) sites become partially occupied to ca. 20% of capacity, with the D3 site falling back to 8% occupancy by 330 °C,

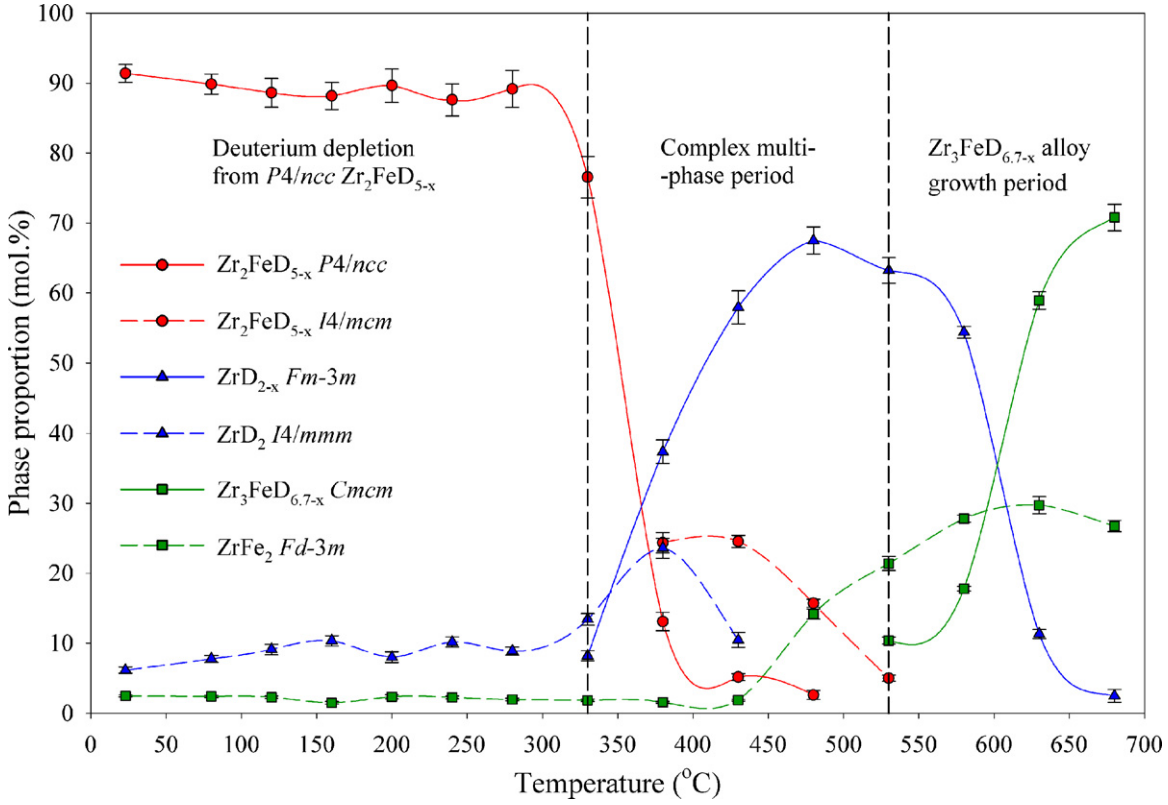

Fig. 4. Crystalline molar phase proportions of all known crystalline phases as a function of temperature from 20 to 680 °C.

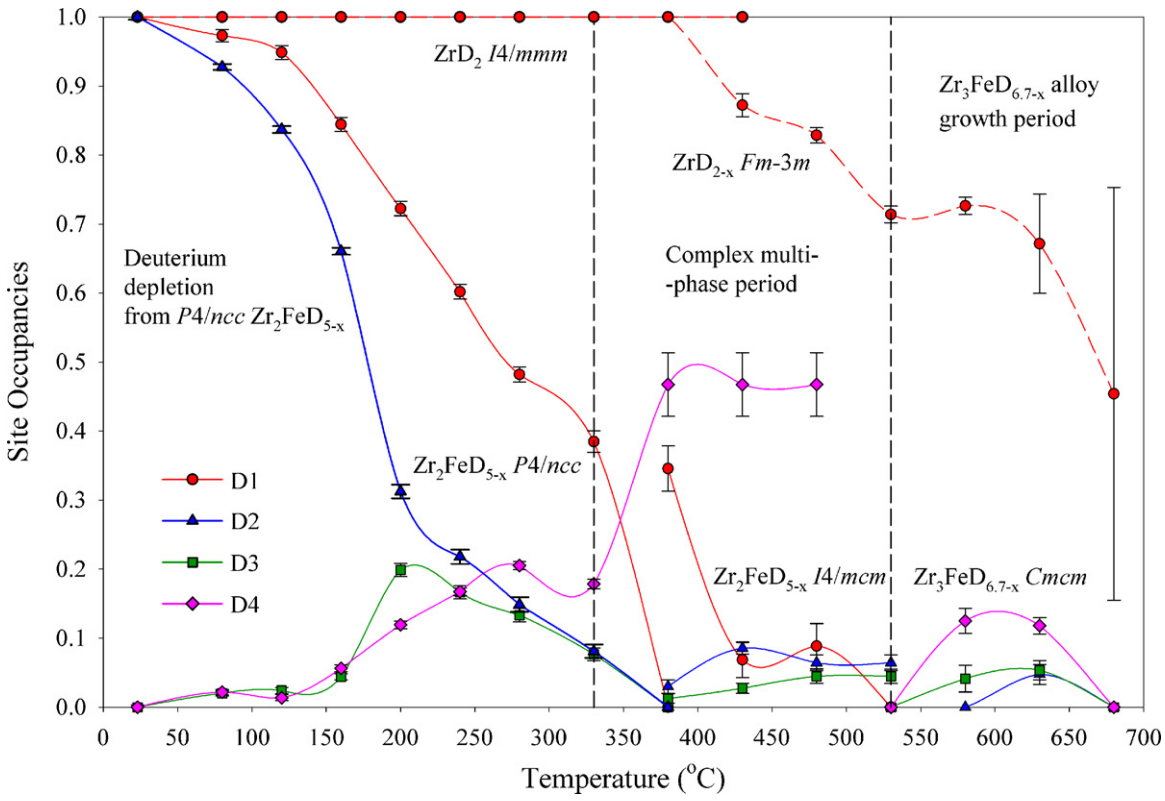

Fig. 5. Deuterium occupancies of all known D containing phases as a function of temperature from 20 to 680 °C.

and the D4 site continuing to increase into the complex multi-phase period. From 280 °C to 330 °C, the molar proportion of the *P*4/*ncc* Zr_2FeD_{5-x} phase is reduced from 89.2% to 76.6%, commensurate with the formation of nanoscopic cubic ZrD_2 by 330 °C (8.2 mol.%), and an increase in the tetragonal ZrD_2 proportion to 13.4 mol.%, and $ZrFe_2$ remaining at ca. 1.8 mol.%. Fig. 6 shows the variation of the *P*4/*ncc* Zr_2FeD_{5-x} lattice parameters. Both the basal and the prismatic unit cell parameters show a smooth decrease up to 330 °C,

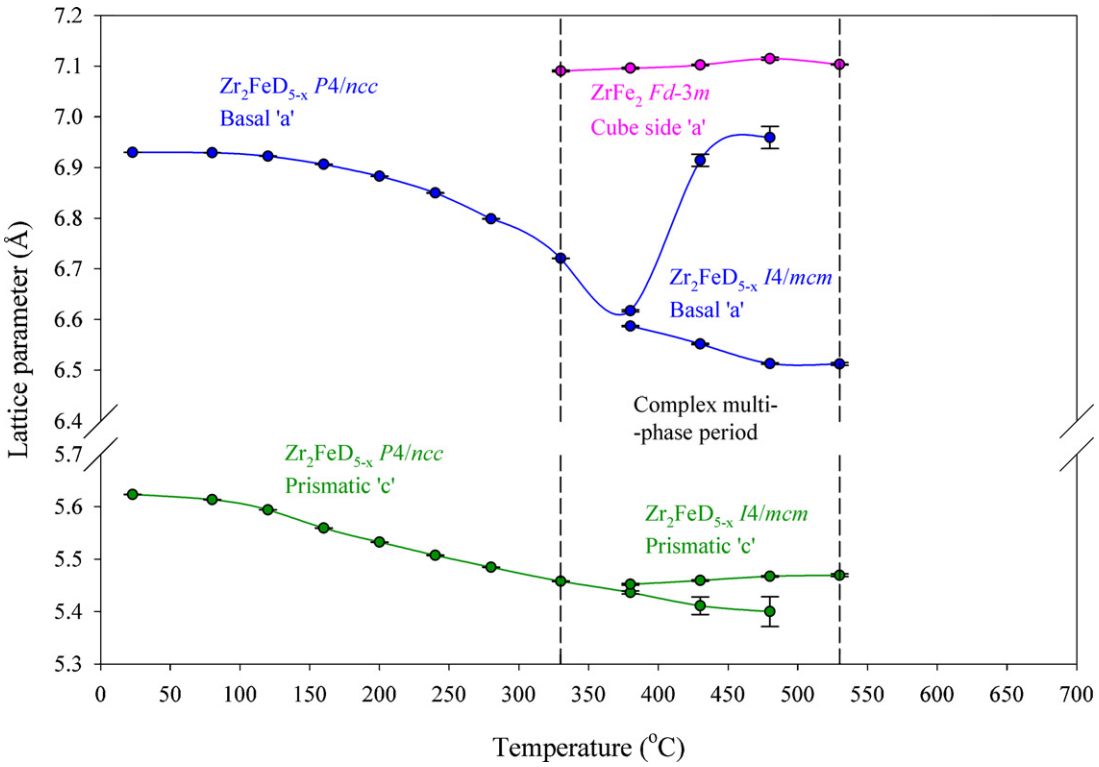

Fig. 6. Variation of the *P*4/*ncc* Zr_2FeD_{5-x} lattice parameters from 20 to 480 °C.

consistent with the continuous loss of D from the cell as a function of temperature. According to QPA of all observed crystalline phases, the temperature range from 20 to 330 °C can be characterised by two reaction types, the first describing the simple loss of D from Zr_2FeD_5 from room temperature up to 280 °C:

$$(20–280\,^{\circ}C)\quad Zr_2FeD_5 \rightarrow Zr_2FeD_{2.35} + 1.33D_2(g) \tag{1}$$

The second reaction describes the formation of nanocrystals of cubic (c) ZrD_2 and an increase in the tetragonal (t) ZrD_2 proportion from 280 to 330 °C, by consumption of a small amount of the *P*4/*ncc* Zr_2FeD_{5-x} phase:

$$(280–330\,^{\circ}C)\quad Zr_2FeD_{2.35} \rightarrow 0.85Zr_2FeD_{1.76} + 0.1ZrD_2 + (c)\,0.05ZrD_2(t) + 0.29D_2(g) \tag{2}$$

It can be noted from reaction (2) that only ca. 93% of the Zr and 85% of the Fe is accounted for. This implies the dispersion of a minor fraction of the sample to an amorphous $Zr_{1-x}Fe_x$ phase. The presence of amorphous $Zr_{1-x}Fe_x$ phases in the sample is discussed below (in Section 3.4) with regard to the total crystalline atom count by QPA.

3.2. Complex multi-phase period from 330 to 530 °C

Inspection of Fig. 4 shows that this period in temperature is strongly multi-phase, and dominated by the appearance and growth of cubic ZrD_2, which at its maximum consumes ca. 2/3rd of the sample. Growth of the alloy phase $ZrFe_2$ also occurs during this period, with the appearance of $Zr_3FeD_{6.7-x}$ by 530 °C. The *P*4/*ncc* Zr_2FeD_{5-x} phase disappears by 480 °C, and formation of the *I*4/*mcm* Zr_2FeD_{5-x} phase occurs at 380 °C, which is also subsumed by 530 °C. Inspection of Fig. 3 suggests that only a minor amount of D comes out of the crystalline phases in the sample between 380 and 480 °C, which is inconsistent with previously reported thermal desorption spectra showing continuous hydrogen release occurring during this period [30]. To follow the behaviour of each phase in this complex region of temperature, we break the discussion into three sections, concerning (i) the tetragonal deuterides *P*4/*ncc* Zr_2FeD_{5-x} and *I*4/*mcm* Zr_2FeD_{5-x}, and their distribution of D sites and unit cell variation, (ii) the formation of significant quantities of the mono deuterides *Fm*$\bar{3}$*m* ZrD_{2-x} and *I*4/*mmm* ZrD_2, and the very broad peak shape of cubic ZrD_2, and (iii) the appearance and growth of the alloy phases *Cmcm* $Zr_3FeD_{6.7-x}$ and *Fd*$\bar{3}$*m* $ZrFe_2$, and the weak occupancy of D in the $Zr_3FeD_{6.7-x}$ phase at high temperature. Concluding these sections, we will discuss the presence of amorphous $Zr_{1-x}Fe_x$ phases in the sample, as indicated by the total crystalline atom count.

3.2.1. Tetragonal deuterides *P*4/*ncc* Zr_2FeD_{5-x} and *I*4/*mcm* Zr_2FeD_{5-x}

From 330 to 380 °C, the occupancies of the D1 (4b Zr_4), D2 (16g = 32m/2 Zr_3Fe) and D3 (16g = 32m/2 Zr_3Fe) sites of the *P*4/*ncc* Zr_2FeD_{5-x} structure are reduced to zero, while the D4 (16g = 16l Zr_4) occupancy rises to a maximum of ca. 46% occupancy, commensurate with a very large reduction in proportion of *P*4/*ncc* Zr_2FeD_{5-x} from 76.5 to 13.1 mol.%. After 480 °C, the *P*4/*ncc* Zr_2FeD_{5-x} phase is no longer visible. The large reduction in *P*4/*ncc* Zr_2FeD_{5-x} content from 330 to 380 °C corresponds to the formation of the *I*4/*mcm* Zr_2FeD_{5-x} phase, and significant rises in proportion of both the cubic and the tetragonal ZrD_2 phases. Fig. 5 shows that the D1 (4b Zr_4) site in the *I*4/*mcm* Zr_2FeD_{5-x} structure shows the highest occupation of ca. 35%, while the only other occupied sites, D2 and D4, are both only weakly occupied at <10%. After 530 °C, the *I*4/*mcm* Zr_2FeD_{5-x} phase is no longer visible. The consumption of *P*4/*ncc* Zr_2FeD_{5-x} (P) from 330 to 380 °C to form the *I*4/*mcm* Zr_2FeD_{5-x} phase (I), and increasing quantities of both the cubic and the tetragonal ZrD_2 phases can be described quantitatively as:

$$(330–380\,^{\circ}C)\quad Zr_2FeD_{1.76}(P) \rightarrow 0.17Zr_2FeD_{1.78} + (P)\,0.32Zr_2FeD_{0.60}(I) + 0.38ZrD_2(c) + 0.13ZrD_2 + (t)\,0.12D_2(g) \tag{3}$$

It can be noted that the discrepancy of Zr and Fe atoms in the total atom count is larger again than reaction (2), with only 75% and 50% of the Zr and Fe accounted for. From 380 to 530 °C, the *I*4/*mcm* Zr_2FeD_{5-x} phase is depleted, and is no longer visible after 530 °C. After 480 °C, the *P*4/*ncc* Zr_2FeD_{5-x} phase is no longer visible, and the proportion of the $ZrFe_2$ alloy phase can be observed to increase at the expense of the *I*4/*mcm* Zr_2FeD_{5-x} phase. The consumption of the majority of the *I*4/*mcm* Zr_2FeD_{5-x} phase from 430 to 530 °C can be described as:

$$(430–530\,^{\circ}C)\quad Zr_2FeD_{0.62}(I) + 0.21Zr_2FeD_{1.78}(P) + 0.43ZrD_2 \rightarrow (t)\,0.20Zr_2FeD_{0.62}(I) + 0.22ZrD_{1.45}(c) + 0.79ZrFe_2 + 0.42Zr_3Fe + 0.71D_2(g) \tag{4}$$

On balance, 95% of the Zr atoms are accounted for, and the Fe atom count has increased by ca. 44%, indicating that crystallisation of an amorphous $Zr_{1-x}Fe_x$ phase has occurred by 530 °C, releasing Fe to assist in the growth of the alloy phases $ZrFe_2$ and Zr_3Fe. Inspection of Fig. 6 shows that the smooth unit cell contraction of the *P*4/*ncc* Zr_2FeD_{5-x} phase up to 380 °C is significantly affected by the presence of other phases in the complex multi-phase period from 330 to 530 °C. While the lattice parameters of the *I*4/*mcm* Zr_2FeD_{5-x} phase can be observed to evolve smoothly from the *P*4/*ncc* Zr_2FeD_{5-x} phase after 380 °C, the basal axis of the *P*4/*ncc* Zr_2FeD_{5-x} phase is significantly stretched to a magnitude similar to the $ZrFe_2$ unit cell dimension, consistent with a strong increase of the $ZrFe_2$ proportion after 430 °C. Both of the tetragonal Zr_2FeD_{5-x} exist up to ca. 500 °C with quite a low D concentration, and the *I*4/*mcm* Zr_2FeD_{5-x} phase is slightly more stable by ca. 50 °C.

3.2.2. Mono deuterides *Fm*$\bar{3}$*m* ZrD_2 and *I*4/*mmm* ZrD_2

The tetragonal *I*4/*mmm* ZrD_2 phase is initially present as a minority phase in the sample after deuteration, at ca. 9 mol.%, and does not show any significant change in proportion until past 280 °C, commensurate with a decrease in the *P*4/*ncc* Zr_2FeD_{5-x} proportion to 76.5 mol.%. The *I*4/*mmm* ZrD_2 phase reaches a maximum of 23.6 mol.% at 380 °C, and its growth occurs at the expense of the *P*4/*ncc* Zr_2FeD_{5-x} phase between 330 and 380 °C according to reaction (3). From 380 to 430 °C, the *I*4/*mmm* ZrD_2 proportion is reduced by 56%, according to:

$$(380–430\,^{\circ}C)\quad ZrD_2(t) + 0.55Zr_2FeD_{1.78}(P) \rightarrow 0.22Zr_2FeD_{1.78} + (P)\,0.87ZrD_{1.75}(c) + 0.44ZrD_2(t) \tag{5}$$

This equation is not balanced, as reactant and product terms have been removed to show only the phase formation contributing to tetragonal *I*4/*mmm* ZrD_2 depletion. The fully balanced 10 term equation shows that 94% of the Zr and 82% of the Fe is accounted for at 430 °C, again suggesting the formation of amorphous $Zr_{1-x}Fe_x$ phases. The tetragonal *I*4/*mmm* ZrD_2 phase does not lose any D at any temperature. The cubic *Fm*$\bar{3}$*m* ZrD_{2-x} phase grows by 20 mol.% between 380 and 430 °C, and is formed directly from depletion of tetragonal *I*4/*mmm* ZrD_2 and *P*4/*ncc* Zr_2FeD_{5-x}. After 430 °C, the tetragonal *I*4/*mmm* ZrD_2 phase is no longer observed. Inspection of Fig. 4 shows that from 430 to 530 °C, the cubic *Fm*$\bar{3}$*m* ZrD_{2-x} phase reaches maximum content where it consumes ca. 2/3rd of the sample at 480 °C. During this period, the *P*4/*ncc* Zr_2FeD_{5-x} and *I*4/*mcm* Zr_2FeD_{5-x} phases are depleted, and $ZrFe_2$ alloy growth starts past 430 °C, and Zr_3Fe can be observed at 530 °C. Growth of the cubic

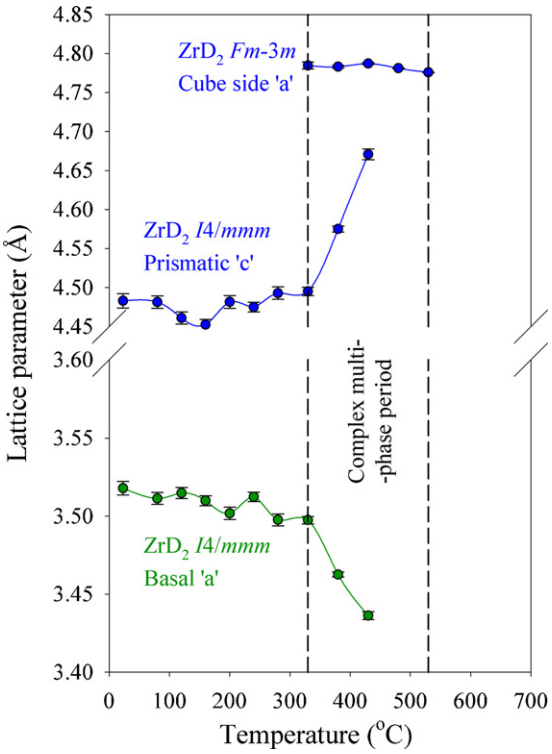

Fig. 7. Variation of the lattice parameters of cubic $Fm\bar{3}m$ ZrD_{2-x} and tetragonal $I4/mmm$ ZrD_2 phases from 20 to 530 °C.

$Fm\bar{3}m$ ZrD_{2-x} phase can be described by reaction (4), where three phases are depleted to form two. From 380 to 530 °C, the D content of the cubic $Fm\bar{3}m$ ZrD_{2-x} phase is reduced to 72.6% (see Fig. 5). Inspection of Fig. 7 shows that the cubic $Fm\bar{3}m$ ZrD_{2-x} unit cell dimension appears little affected by this D loss (only a very small compression can be observed from 430 °C onward, consistent with D loss), and the cell may be dilated in the presence of other phases. In contrast, the tetragonal $I4/mmm$ ZrD_2 phase shows distinct basal compression and prismatic expansion from 330 to 430 °C, with Δa ca. −0.06 Å, and Δc ca. +0.18 Å, an order of magnitude difference compared to the 0.01 Å change in the cube side. As such, the cubic $Fm\bar{3}m$ ZrD_{2-x} phase is likely mechanically stiffer than the tetragonal $I4/mmm$ ZrD_2 phase, also indicated by the c-axis of the tetragonal $I4/mmm$ ZrD_2 phase being stretched toward the cube side, which is the only unit cell dimension (c = 4.5730 Å) that is coherently close in dimension to the cubic $Fm\bar{3}m$ ZrD_{2-x} unit cell (a = 4.7843 Å) in the 330–430 °C range. A mechanical couple between the tetragonal and cubic ZrD_2 phases is also implied by the growth of cubic ZrD_{2-x} from tetragonal ZrD_2 according to reactions (4) and (5). The contribution from the initially very broad reflections of the cubic $Fm\bar{3}m$ ZrD_2 phase are shown in a zoomed section of the neutron diffraction pattern at 380 °C, over 40–90° 2θ, in Fig. 8. By 530 °C, the cubic $Fm\bar{3}m$ ZrD_{2-x} reflections have sharpened considerably. Lineshape analysis suggests the cubic $Fm\bar{3}m$ ZrD_2 initially forms on the 15 nm length scale, which by 580 °C has increased to >100 nm. After 530 °C, the cubic $Fm\bar{3}m$ ZrD_{2-x} phase proportion begins to rapidly decrease.

3.2.3. Alloy phases Cmcm Zr_3Fe and $Fm\bar{3}m$ $ZrFe_2$

The cubic alloy $ZrFe_2$ is present as a minority phase of ca. 2 mol.% in the original arc melted sample, and is present in the sample over the entire temperature interval of 20–680 °C. Fig. 4 shows $ZrFe_2$ growth begins after 430 °C, and the growth of $ZrFe_2$ from 430 to 530 °C follows reaction (4). As the tetragonal $I4/mmm$ ZrD_2 phase is likely mechanically coupled and directly consumed by the cubic $Fm\bar{3}m$ ZrD_{2-x} phase, growth of $ZrFe_2$ occurs directly by depletion of the $P4/ncc$ Zr_2FeD_{5-x} and the $I4/mcm$ Zr_2FeD_{5-x} phases, mostly the $I4/mcm$ Zr_2FeD_{5-x} phase, as the $P4/ncc$ Zr_2FeD_{5-x} proportion remains below ca. 5 mol.% from 430 to 480 °C. From 480 to 530 °C, growth of $ZrFe_2$ is mostly from $I4/mcm$ Zr_2FeD_{5-x} depletion. From the atom balance of reaction (4), it is also likely that an amorphous $Zr_{1-x}Fe_x$ phase is crystallising up to 530 °C, and an excess of Fe from this amorphous phase may also contribute to the growth of $ZrFe_2$. From 480 to 530 °C, the proportion of the cubic $Fm\bar{3}m$ ZrD_{2-x} phase decreases by ca. 4 mol.%, and by 530 °C, the orthorhombic $Cmcm$ Zr_3Fe phase can be observed in the neutron diffraction pattern at a proportion of 10.4 mol.%. From 480 to 530 °C, the growth of $ZrFe_2$

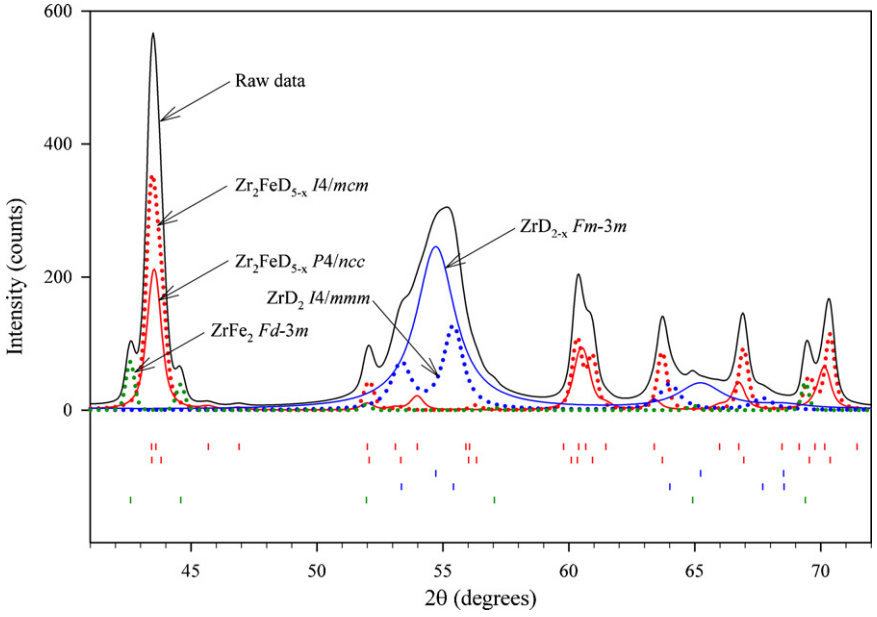

Fig. 8. Neutron diffraction pattern at 380 °C zoomed from 53 to 73° 2θ, showing the very broad reflections from cubic $Fm\bar{3}m$ ZrD_{2-x}. Reflection markers from top to bottom are $P4/ncc$ Zr_2FeD_{5-x}, $I4/mcm$ Zr_2FeD_{5-x}, cubic $Fm\bar{3}m$ ZrD_{2-x}, tetragonal $I4/mmm$ ZrD_2 and $ZrFe_2$.

and Zr_3Fe alloy phases can be described as:

$$(480\text{–}530\,^{\circ}\text{C})\quad Zr_2FeD_{0.62}(\text{I}) + 0.17Zr_2FeD_{1.78} + (\text{P})\,4.29ZrD_{1.66}(\text{c}) \rightarrow 0.32Zr_2FeD_{0.62}(\text{I}) + 4.02ZrD_{1.45} + (\text{c})\,0.46ZrFe_2 + 0.42Zr_3Fe \quad (6)$$

Reactant terms have been removed to show only the phase formation contributing to the growth of $ZrFe_2$ and Zr_3Fe, the majority of which occurs by depletion of the *I*4/*mcm* Zr_2FeD_{5-x} phase, with a minor amount of Zr being sourced from cubic ZrD_{2-x}. The atom balance indicates a ca. 6% increase in Zr and a 47% increase in Fe, again, consistent with the ongoing crystallisation of an amorphous $Zr_{1-x}Fe_x$ phase. The significant proportion of ca. 10 mol.% Zr_3Fe suggests it has nucleated well before 530 °C.

3.3. Zr_3Fe alloy growth period from 530 to 680 °C

This high temperature period is well characterised by the dominant growth of the alloy phase Zr_3Fe (see Fig. 4), a moderate rise in $ZrFe_2$ proportion, and strong depletion of cubic *Fm*$\bar{3}$*m* ZrD_{2-x}. Inspection of Fig. 5 shows that the Zr_3Fe is weakly occupied by D, which can only be sourced from the cubic *Fm*$\bar{3}$*m* ZrD_{2-x} phase, suggesting a morphology of intimate mechanical contact between the phases, allowing D diffusion that is not blocked by the presence of $ZrFe_2$. There are four D sites available in the $Zr_3FeD_{6.7}$ structure [30], D1 (4c Zr_3Fe_2), D2 (8f Zr_3Fe), D3 (8f Zr_4), and D4 (8f Zr_4). The D3 and D4 sites show weak occupancy <12% from 580 to 630 °C and <5% occupancy of the D2 site at 630 °C. This is consistent with [30], where typically only the Zr_4 tetrahedra are occupied at weak D concentrations. The trigonal bypyramid Zr_3Fe_2 is not occupied. The Zr_3Fe structure does not hold any D at 680 °C, and by this temperature, the cubic *Fm*$\bar{3}$*m* ZrD_{2-x} proportion is reduced to ca. 2.5 mol.%. From 530 to 580 °C, $ZrFe_2$ and $Zr_3FeD_{6.7-x}$ growth occurs mostly from the cubic *Fm*$\bar{3}$*m* ZrD_{2-x} phase according to:

$$(530\text{–}580\,^{\circ}\text{C})\quad ZrD_{1.44}(\text{c}) + 0.08Zr_2FeD_{0.62}(\text{I}) \rightarrow 0.86ZrD_{1.45} + (\text{c})\,0.10ZrFe_2 + 0.12Zr_3FeD_{0.34} + 0.38D_2(\text{g}) \quad (7)$$

This equation has reactant and product terms removed to show only those phases contributing to $ZrFe_2$ and $Zr_3FeD_{6.7-x}$ growth (the D content in the equation has been balanced to emphasise D release from the sample). On balance, there is a 9% and 21% increase in Zr and Fe respectively. This indicates that even at 580 °C, there is still amorphous $Zr_{1-x}Fe_x$ crystallising. After 580 °C, there is little change in the $ZrFe_2$ proportion, and the growth of $Zr_3FeD_{6.7-x}$ can be directly attributed to cubic *Fm*$\bar{3}$*m* ZrD_{2-x} depletion as:

$$(580\text{–}680\,^{\circ}\text{C})\quad ZrD_{1.44}(\text{c}) \rightarrow 0.05ZrD_{1.34}(\text{c}) + 0.97Zr_3Fe + 0.69D_2(\text{g}) \quad (8)$$

Reactant and product terms are removed to show the phases contributing to Zr_3Fe growth. Here we have the strongest indication yet of non-crystalline phases in the sample crystallising and releasing atoms to contribute to the growth of existing crystalline phases, with a 44% and 41% increase in the Zr and Fe atom count respectively. At 680 °C, we do not yet observe the formation of Zr_2Fe, which is below the temperature at which it is observed in the binary phase diagram, 780 °C [14]. Fig. 9 shows the variation in unit cell parameters of $ZrFe_2$ and $Zr_3FeD_{6.7-x}$ as a function of temperature from 530 to 680 °C. The absolute change in magnitude of these lattice parameters is minor for example compared to the variation of *P*4/*ncc* Zr_2FeD_{5-x} lattice parameters in Fig. 6. However, all metrics of the $Zr_3FeD_{6.7-x}$ phase can be observed to rise and fall, commensurate with the weak rise and fall in D occupancy across the D2–D4 sites. In contrast, the $ZrFe_2$ unit cell displays a normal rise, consistent with typical thermal expansion in the absence of D.

3.4. Amorphous $Zr_{1-x}Fe_x$ phases during thermal disproportionation of Zr_2FeD_{5-x}

For reactions (2)–(8) described above, we have consistently observed a discrepancy in the balance of Zr and Fe atoms. For reactions (2), (3) and (5) covering 280–430 °C, we observe a loss of Zr and Fe atoms from the observed crystalline phases in the sample. For reactions (4) and (6)–(8) covering 430–680 °C, we observe a gain in Zr and Fe atoms. Fig. 10 shows the total atom count of Zr, Fe and D across the entire temperature range of Zr_2FeD_5 disproportionation. Table 1 also summarises the change in composition of all crystalline phases, the temperature range in which they are stable, and what their unit cell dimensions range over. Inspection of Fig. 10 shows the temperature range over which Fe recovery occurs is very large, covering 200 °C from 430 to 630 °C. The large temperature range of recovery suggests that several amorphous (a-) $Zr_{1-x}Fe_x$ compositions may be present in the sample, and indeed, when summing the discrepancy from the total (fully crystallised) atom count at 680 °C, we can infer that a-$Zr_{71}Fe_{29}$ must be present in the originally arc melted sample, and that a-$Zr_{56}Fe_{44}$ formation occurs from 280 to 430 °C. It is not unreasonable to expect an amorphous composition in an inhomogenous arc melt close to the Zr_2Fe composition. Nor is it surprising to expect the formation of a-$Zr_{1-x}Fe_x$ phases, particularly when the crystalline phases in the phase transition all have such dissimilar lattice parameters. The most plausible explanation is that the domination of the cubic *Fm*$\bar{3}$*m* ZrD_{2-x} phase in the multi-phase region from 330 to 530 °C is the origin of considerable lattice parameter misfit with other phases, resulting in the spread of dislocations and interfacial growth of a-$Zr_{1-x}Fe_x$ phases. There is a significant resolvable strain component in the cubic *Fm*$\bar{3}$*m* ZrD_{2-x} lineshape when it is initially forming, and dislocation loop punching is likely, as is observed for needle like ZrH_x precipitates [31]. As such, we would expect considerable microstructure commensurate with ZrD_{2-x} nucleation, and the formation of a-$Zr_{1-x}Fe_x$ phases along the grain boundaries. Such features obviously suggest the use of transmission electron microscopy (TEM) to be vindicated.

The total atom count of D also suggests the presence of D in non-crystalline phases. Fig. 3 shows the release of D from crystalline $Zr_{1-x}Fe_xD_y$ phases is minimal in the 380–480 °C temperature range. The thermal desorption data in [30] clearly show deuterium evolution from Zr_2FeD_5 disproportionation in this temperature range. An explanation can be found in [20], where it has been observed that 0.2–0.7 wt.%H can be solved into a-$Zr_{67}Fe_{33}$. The presence of H in a-$Zr_{67}Fe_{33}H_x$ increases T_{cryst} by ca. 40 °C. According to the concentration dependent crystallisation temperatures reported in [10], a-$Zr_{71}Fe_{29}$ will begin crystallising at ca. 365 °C, or ca. 405 °C for a-$Zr_{71}Fe_{29}D_x$, assuming no significant isotope effect. These crystallisation temperatures fall in the 380–480 °C range, and the obvious inference is that D released from the sample in this temperature range can come from a-$Zr_{71}Fe_{29}D_x$ present in the initially deuterated arc melt. Crystallisation of a-$Zr_{71}Fe_{29}D_x$ beginning at ca. 405 °C is also consistent with the Fe recovery observed from ca. 430 °C onward. The crystallisation of a-$Zr_{71}Fe_{29}$ and a-$Zr_{71}Fe_{29}D_x$ is shown by the dashed lines in Fig. 10. As such, the complex crystalline multi-phase period from 330 to 530 °C is further complicated by the formation of a-$Zr_{56}Fe_{44}$ from 280 to 430 °C, and the crystallisation of a-$Zr_{71}Fe_{29}D_x$ and release of D from ca. 405 °C. Zr and Fe recovery after 530 °C is also consistent with the crystallisation of a-$Zr_{56}Fe_{44}$ starting at ca. 535 °C according to [10]. It is also clear that the boundaries for crystallisation of a-$Zr_{71}Fe_{29}$ and a-$Zr_{56}Fe_{44}$ are very close in temperature to the beginning (330 °C) and end (530 °C) respectively of the complex multi-phase period, and

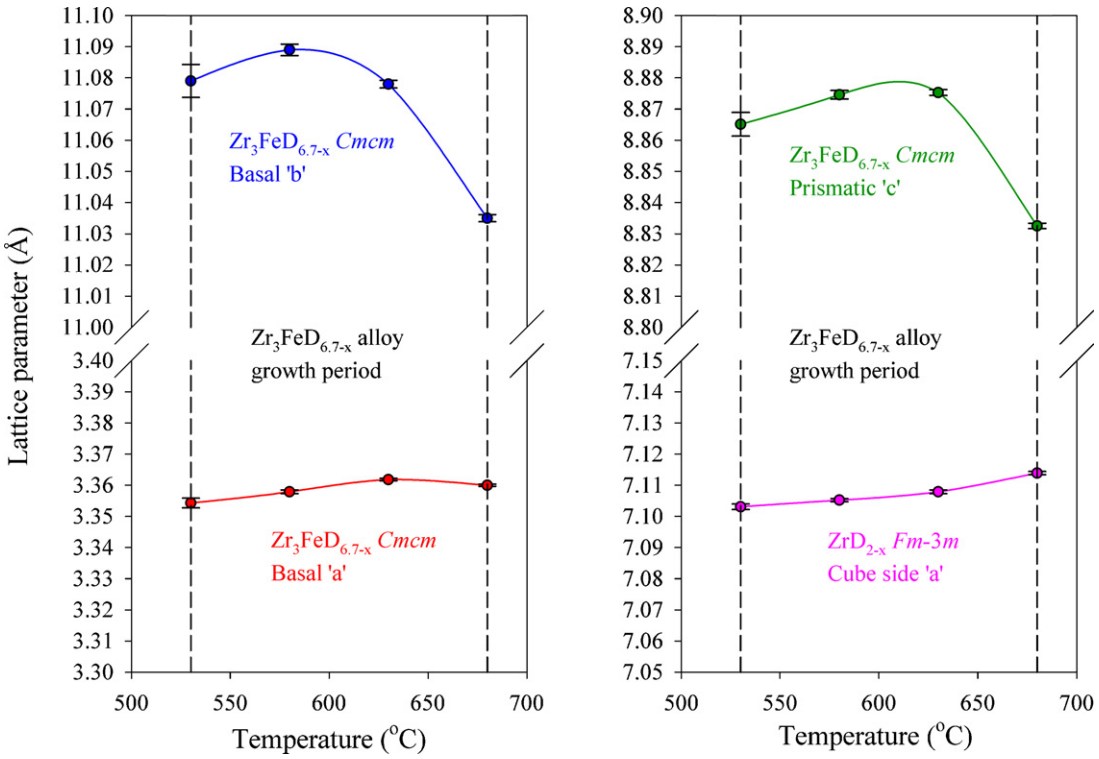

Fig. 9. Variation of the lattice parameters of $Zr_3FeD_{6.7-x}$ and $ZrFe_2$ from 530 to 680 °C.

the presence of a-$Zr_{1-x}Fe_x$ phases may have significant influence on the temperature dependence of the crystalline disproportionation of Zr_2FeD_5. We have not found reports describing a-$Zr_{1-x}Fe_x$ phases in the literature concerning Zr_2FeD_5 disproportionation, however, this is the first accurate quantitative description of the phase transition. Clearly the initial state of the prepared Zr_2Fe alloy is critical in this regard, and should be carefully assessed for the presence of a-$Zr_{1-x}Fe_x$ phases by TEM. Regardless of the initial sample state, it appears that a-$Zr_{1-x}Fe_x$ phase formation occurs naturally after 330 °C as part of the Zr_2FeD_5 disproportionation process. This mechanism should be verified and studied further by TEM.

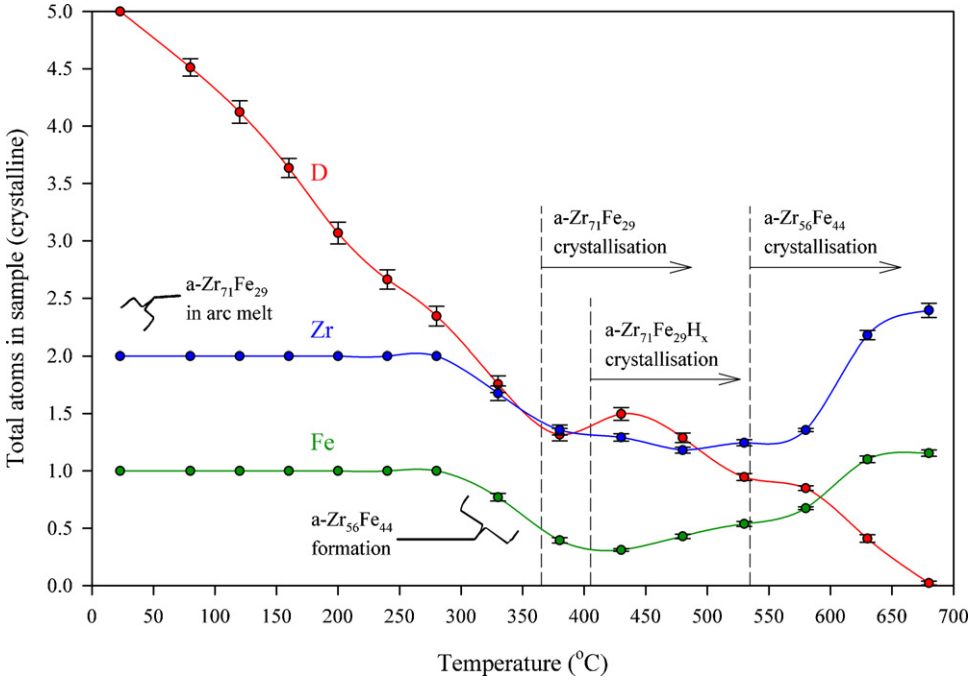

Fig. 10. Total atom count from all known crystalline phases as a function of temperature from 20 to 680 °C. T_{cryst} of a-$Zr_{71}Fe_{29}$, a-$Zr_{71}Fe_{29}D_x$ and a-$Zr_{56}Fe_{44}$ are shown for reference.

Table 1
A summary of all crystalline phases occurring during the disproportionation of Zr_2FeD_5, showing from top to bottom, changes in deuterium composition, the temperature range in which they are stable, and what their unit cell dimensions range over.

Zr_2FeD_{5-x} *P4/ncc*	Zr_2FeD_{5-x} *I4/mcm*	ZrD_2 *I4/mmm*	ZrD_{2-x} *Fm$\bar{3}$m*	$ZrFe_2$ *Fd$\bar{3}$m*	$Zr_3FeD_{6.7-x}$ *Cmcm*
$Zr_2FeD_5 \rightarrow Zr_2FeD_{1.76}$	$Zr_2FeD_{0.62} \rightarrow Zr_2FeD_{0.60}$	ZrD_2	$ZrD_2 \rightarrow ZrD_{0.91}$	$ZrFe_2$	$Zr_3FeD_{0.34} \rightarrow Zr_3Fe$
20–480 °C	380–530 °C	Minor 20–330 °C Major 330–430 °C	330–680 °C	Minor 20–430 °C Major 430–680 °C	530–680 °C
a = 6.617(2)–6.95(2) Å	a = 6.512(2)–6.586(1) Å	a = 3.436(2)–3.517(4) Å	a = 4.755(5)–4.784(5) Å	a = 7.087(1)–7.114(3) Å	a = 3.354(1)–3.3618(4) Å
–	–	–	–	–	b = 11.035(1)–11.089(2) Å
c = 5.39(3)–5.6232(2) Å	c = 5.451(1)–5.469(3) Å	c = 4.452(6)–4.670(6) Å	–	–	c = 8.8325(8)–8.8753(9) Å

4. Conclusion

The disproportionation of Zr_2FeD_5 is a considerably complex phase transition, characterised as a function of temperature by three distinct events, the initial depletion of D from *P*4/*ncc* Zr_2FeD_{5-x} to 330 °C, a complex multi-phase period from 330 to 530 °C dominated by the growth of cubic *Fm*$\bar{3}$*m* ZrD_{2-x}, and the subsequent growth of $Zr_3FeD_{6.7-x}$ from 530 to 680 °C. Accompanying these crystalline transitions, our quantitative analysis infers two distinct crystallisation events, from a-$Zr_{71}Fe_{29}$ and a-$Zr_{56}Fe_{44}$ which correspond closely to the low and high temperature boundaries of the complex multi-phase region. Our QPA indicates that a-$Zr_{56}Fe_{44}$ has formed naturally as part of the phase transition, likely a consequence of incoherent matching of lattice parameters to the dominant cubic *Fm*$\bar{3}$*m* ZrD_{2-x} phase. TEM is the obvious choice to verify the a-$Zr_{1-x}Fe_x$ formation at high temperature, by studying samples quenched from above ca. 330 °C. Arc melted crystalline Zr_2Fe alloys should also be examined by TEM for the presence of amorphous $Zr_{1-x}Fe_x$ phases.

References

[1] J. Prigent, M. Latroche, E. Leoni, V. Rohr, J. Alloys Compd., in press, doi:10.1016/j.jallcom.2010.10.199.
[2] S. Zalkind, M. Nahmani, N. Shamir, J. Alloys Compd. 501 (2010) 221.
[3] K.M. Fox, J. Ceram. Process. Res. 10 (2009) 705.
[4] M. Coleman, D. Chandra, J. Wermer, T. Udovic, in: D. Chandra, R.G. Bautista, L. Schlapbach (Eds.), Advanced Materials for Energy Conversion II, The Minerals, Metals & Materials Society, Warrendale, 2004, pp. 429–435.
[5] S. Fukada, Y. Toyoshima, M. Nishikawa, Fusion Eng. Des. 49–50 (2000) 805.
[6] S. Fukada, K. Tokunaga, M. Nishikawa, Fusion Eng. Des. 36 (1997) 471.
[7] S. Fukada, M. Nishikawa, J. Alloys Compd. 234 (1996) L7.
[8] R. Janot, M. Latroche, A. Percheron-Guegan, Mater. Sci. Eng. B 123 (2005) 187.
[9] D. Mishra, A. Perumal, A. Srinivasan, J. Phys. D Appl. Phys. 41 (2008) 215003.
[10] A.W. Weeber, H. Bakker, Physica B 153 (1988) 93.
[11] X.D. Liu, X.B. Liu, Z. Altounian, J. Non-Cryst. Solids 351 (2005) 604.
[12] P.T. Korelis, A. Liebig, M. Bjorck, B. Hjorvarsson, H. Lidbaum, K. Leifer, A.R. Wildes, Thin Solid Films 519 (2010) 404.
[13] P. Sharma, H. Kimura, A. Inoue, Phys. Rev. B 78 (2008) 134414.
[14] F. Stein, G. Sauthoff, M. Palm, J. Phase Equilib. 23 (2002) 480.
[15] A. Inoue, Acta Mater. 48 (2000) 279.
[16] F. Aubertin, U. Gosner, S.J. Campbell, J. Phys. F Met. Phys. 14 (1984) 2213.
[17] P. Raj, P. Suryanarayana, A. Sathyamoorthy, K. Shashikala, R.M. Iyer, J. Alloys Compd. 178 (1992) 393.
[18] V.A. Yartys, H. Fjellvag, B.C. Hauback, A.B. Riabov, J. Alloys Compd. 274 (1998) 217.
[19] Z. Altounian, E. Batalla, J.O. Strom-Olsen, J.L. Walter, J. Appl. Phys. 61 (1986) 149.
[20] T. Himitliiska, T. Spassov, J. Therm. Anal. Calorim. 96 (2009) 347.
[21] Y. Filinchuk, K. Yvon, Inorg. Chem. 44 (2005) 8191.
[22] M.H. Sorby, H. Fjellvag, B.C. Hauback, J. Alloys Compd. 394 (2005) 107.
[23] A. Nobile, W.C. Mosley, J.S. Holder, K.N. Brooks, J. Alloys Compd. 206 (1994) 83.
[24] V.A. Yartys, I.Yu. Zavaliy, A.B. Riabov, P.W. Guegan, J.C. Clarke, I.R. Harris, B.C. Hauback, H. Fjellvag, in: T.O. Saetre (Ed.), Proceedings of the International Symposium HYPOTHESIS II, Kluwer Academic, Netherlands, 1998, pp. 303–314.
[25] V.A. Yartys, H. Fjellvag, B.C. Hauback, A.B. Riabov, M.H. Sorby, J. Alloys Compd. 278 (1998) 252.
[26] V.A. Yartys, O. Gutfleisch, V.V. Panasyuk, I.R. Harris, J. Alloys Compd. 253–254 (1997) 128.
[27] M. Hara, R. Hayakawa, Y. Kaneko, K. Watanabe, J. Alloys Compd. 352 (2003) 218.
[28] B.C. Hauback, H. Fjellvag, O. Steinsvoll, K. Johansson, O.T. Buset, J. Jorgensen, J. Neutron Res. 8 (2000) 215.
[29] B.A. Hunter, Comm. Powder Diffr. Newsl. 20 (1998) 21.
[30] V.A. Yartys, H. Fjellvag, I.R. Harris, B.C. Hauback, A.B. Riabov, M.H. Sorby, I.Yu. Zavaliy, J. Alloys Compd. 293–295 (1999) 74.
[31] J.S. Bradbrook, G.W. Lorimer, N. Ridley, J. Nucl. Mater. 42 (1972) 142.